Low-lying levels in ^{57}Cu and the *rp* process

X. G. Zhou, H. Dejbakhsh, C. A. Gagliardi, J. Jiang, L. Trache,* and R. E. Tribble
Cyclotron Institute, Texas A&M University, College Station, Texas 77843
(Received 10 July 1995)

The level scheme of ^{57}Cu is investigated via the ^{1}H(^{58}Ni,^{57}Cu-γ)2*n* reaction by using the recoil mass spectrometer MARS at the Texas A&M Cyclotron Institute. Three low-lying excited states are observed in ^{57}Cu at 1028 ± 4, 1106 ± 4, and 2398 ± 10 keV. The results are compared with well known excited states of the mirror nucleus ^{57}Ni. The measured excited states of ^{57}Cu allow recalculation of the astrophysical reaction rate for the stellar radiative proton capture reaction ^{56}Ni$(p,\gamma)^{57}$Cu.

PACS number(s): 21.10.Hw, 23.20.Lv, 26.20.+f, 27.40.+z

I. INTRODUCTION

In the naive shell model, the nucleus ^{57}Cu consists of a single proton outside the doubly magic ^{56}Ni core with $N=Z=28$. This simple structure permits far more accurate model calculations than are possible in the middle of a nuclear shell. In particular, a comparison of the low-lying levels of ^{57}Cu with the well-determined excited states of its mirror nucleus ^{57}Ni is important for studying the charge symmetry of the nucleus.

The structure of ^{57}Cu also plays a key role in the nucleosynthesis of heavy proton-rich nuclei. The primary mechanism for producing such nuclei is the *rp* process, which is believed to be important in the dynamics of collapsing supermassive stars and x-ray bursts [1]. Except at the highest temperatures, the stability and long half-life of ^{56}Ni imply that heavier nuclei may be produced only after a ^{56}Ni(p,γ) ^{57}Cu reaction. The rate of this reaction is due almost entirely to the first four resonances. Thus, it is very sensitive to the location and structure of the low-lying states of ^{57}Cu. Relatively small changes in the binding and excitation energies result in significant modifications of the predictions for the synthesis of proton-rich isotopes with $A>56$ and possibly for the time evolution of cosmic x-ray bursts. For a recent detailed discussion of the *rp* process reaction chains, see Ref. [2].

The only previous experimental data available about the low-lying excited states of ^{57}Cu are from Refs. [3,4], where several excited states were observed, but only a single state was seen below an excitation energy of 2.5 MeV. The suggestion was made in Ref. [3] that this single peak, at an excitation energy of 1040 keV, contained two unresolved states, the analogs of the 768 keV $\frac{5}{2}^-$ and 1113 keV $\frac{1}{2}^-$ states in ^{57}Ni.

In this paper, we present results for the first in-beam γ-ray spectroscopy study of ^{57}Cu, which allows us to determine the excitation energies for the first three low-lying excited states of ^{57}Cu. We then utilize a particle-core coupling model to estimate the proton- and gamma-decay widths necessary to calculate the stellar reaction rate of the radiative proton capture reaction ^{56}Ni$(p,\gamma)^{57}$Cu in the temperature range of interest for the *rp* process.

The experimental setup and procedures are described in Sec. II. In Secs. III and IV, we discuss the data analysis and level assignments. Finally, the implications of these measurements for the ^{56}Ni$(p,\gamma)^{57}$Cu reaction are described in Sec. V.

II. EXPERIMENTAL DETAILS

^{57}Cu was produced in the inverse reaction ^{1}H(^{58}Ni, ^{57}Cu)2*n*, with a 31 MeV/nucleon ^{58}Ni beam from the Texas A&M K500 Cyclotron incident on a 14 mg/cm^2 thick polyethylene target. At this energy, the reaction products were emitted in a small forward angle, and most were fully stripped. They were captured by the first quadrupole doublet of the Texas A&M Momentum Achromat Recoil Spectrometer, MARS, with essentially 100% efficiency. The MARS spectrometer physically separates ions of different mass-to-charge (M/Q) ratio at its focal plane. This provides an easy way of identifying the ^{57}Cu nuclei, because ^{57}Cu^{29+} has the smallest M/Q ratio of any ion observed in this experiment. A detailed description of MARS is given in Refs. [5,6]. It uses a unique optical design utilizing two dispersive planes to combine a momentum achromat with a recoil mass spectrometer. This configuration makes MARS applicable to a broad range of experiments, especially those using inverse kinematics at 0°. The first part of MARS, consisting of three quadrupole and two dipole magnets, provides the momentum achromat. The reaction products and the primary beam were captured and focused by a quadrupole doublet and were separated by the first dipole according to their magnetic rigidities. The incident beam was then blocked by a momentum selection slit positioned at an intermediate focal plane near the entrance of the third quadrupole magnet. This slit also stopped many of the ^{58}Cu nuclei produced at the target, while allowing essentially all the ^{57}Cu nuclei to pass. Following the achromatic section of MARS, the recoils were dispersed vertically by a velocity filter. They were then bent up by the third dipole and focused by the final two quadrupoles. This provided a first order M/Q mass focus with a resolution of nearly 1 part in 300. Thus, clean particle identification was straightforward.

We used a 5 × 5 cm^2, 1000 μm thick position sensitive Si strip detector [7] at the MARS focal plane for particle

*Permanent address: Institute of Atomic Physics, Bucharest, Romania.

detection. Measurements of total energy and position were made when each recoil ion stopped. A collimating slit was placed in front of the strip detector to stop some of the recoil ions with $M/Q = 2$ and all of the recoil ions with $M/Q > 2$. With this slit in place, the typical particle rate was 500 Hz with a ^{58}Ni beam current of 5 e nA. Further details regarding recoil identification may be found in Ref. [8].

Prompt γ rays were detected around the target chamber in an array of seven BGO-shielded HPGe detectors of 20% efficiency with a peak/total ratio of 0.43 [9]. We placed our Ge detectors in two rings, with four of them at an angle of 155° and three at 120° with respect to the incident beam. We chose to place the γ detectors in the backward direction to minimize the neutron flux to which they were exposed. This also permitted us to maximize the acceptance solid angle of MARS by locating the target near the entrance to the first MARS quadrupole magnet. To limit the Doppler broadening associated with the high speed of the recoils ($\beta \approx 0.24$), the Ge detectors were collimated with 4.5 cm thick Pb absorbers. Rectangular collimators, oriented with their long sides perpendicular to the reaction plane, were used to balance the competing needs to minimize Doppler broadening and maximize detection efficiency. The sizes were chosen to provide a peak width of less than 10 keV for 1 MeV γ rays radiated from the moving source. The observed peaks were wider than this, however, due to the finite velocity spread associated with recoils decaying at different depths in the polyethylene target. Energy calibrations were done several times during and at the end of the experiment with a ^{152}Eu source placed in the center of the target chamber. Compton suppression for the Ge detectors and the coincidence between particles identified at the MARS focal plane and γ rays observed at the target were made by using commercially available electronic units. The seven Ge energy signals were fed into ORTEC 413 CAMAC analog-to-digital converters (ADC's). The LAMPF Q system was used for data acquisition. A total of 0.8×10^6 recoil-γ coincident events were recorded to tape.

III. DATA ANALYSIS AND RESULTS

To identify the low-lying excited states of ^{57}Cu, we first created particle-gated γ-ray spectra from the seven Ge detectors for each run. Then two summed spectra were created, one for each of the detector angles, by adding the individual spectra from the various Ge detectors and runs after gain match and Doppler shift corrections were made. Because the absolute velocity of the recoil nuclei and the angles of the Ge detectors to the beam were not precisely known, the corrections for Doppler shift were determined in a relative way. As noted above, the slit in front of the Si detector was positioned so that some of the $N=Z$ recoil nuclei would be visible. We recorded $N=Z$ particle-γ coincidence events concurrently with the ^{57}Cu data. For each of the seven Ge detectors, the Doppler shifts for the $N=Z$ recoils were obtained from a comparison of the known γ rays at 375.9, 509.3, and 937.2 keV in ^{54}Co and 203.0, 444.6, and 848.5 keV in ^{58}Cu with our observed γ-ray energies. Given the run-by-run statistics, not every line was visible in every detector-run combination. We also observed the 1223 keV γ ray in ^{56}Ni, but we did not use it in the Doppler shift calibration because its line shape appeared distorted, possibly by a second unresolved γ ray. Figure 1 shows the summed γ-ray spectrum from the four 155° detectors, gated on $N=Z$ recoil nuclei, after the Doppler shift correction has been applied. The 511 keV positron annihilation γ ray and the 846.8 keV γ ray associated with the decay of the first excited state in ^{56}Fe are also observed in Fig. 1. The excited state of ^{56}Fe was populated by the bombardment of a steel mounting plate and the first MARS quadrupole magnet by the fast neutrons produced in the reactions leading to the $N=Z$ recoils. Note that these two peaks do not appear at the ''correct'' energies because they were emitted from stationary sources, and their positions were moved in our procedure to correct for the Doppler shift. The additional lines seen in Fig. 1 are all due to weak transitions in the $N=Z$ nuclei or inelastic neutron scattering on Ge.

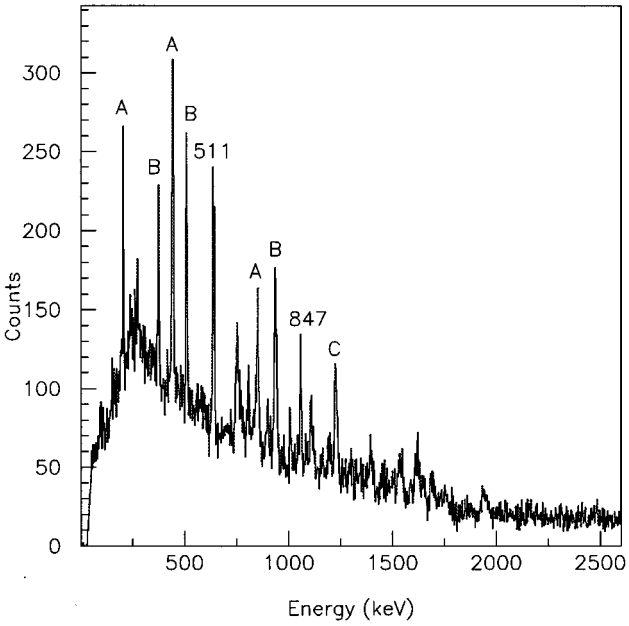

FIG. 1. The summed γ-ray spectrum from the 155° detectors, gated on $N=Z$ recoil nuclei, after gain matching and Doppler shift corrections have been applied. The γ-ray lines labeled A, B, and C represent transitions in ^{58}Cu, ^{54}Co, and ^{56}Ni, respectively. The 511 keV line is from annihilation radiation, while the 847 keV line is from ^{56}Fe. See text for details.

The Doppler shift for ^{57}Cu events was derived by calculating the average velocity of ^{57}Cu relative to the speed of the $N=Z$ ions. We estimate that the velocity of the ^{57}Cu recoil nuclei was 1.8% faster than that of the $N=Z$ species, assuming a constant magnetic rigidity for all particles passing through the momentum selection slit mentioned above. The Doppler shift was adjusted for ^{57}Cu events accordingly. The summed spectra from the 155° and 120° detectors, gated on ^{57}Cu recoil nuclei, are shown in Figs. 2 and 3, respectively, after the correction for Doppler shift. ^{57}Cu excited states are observed at 1027, 1106, and 2399 keV in the 155° detectors and at 1029, 1107, and 2397 keV in the 120° detectors. The 511 and 846.8 keV γ rays are seen in these two figures, too. They are fragmented in Fig. 3 because the three 120° Ge detectors were not aligned at the same angle, and so they had slightly different Doppler shift cor-

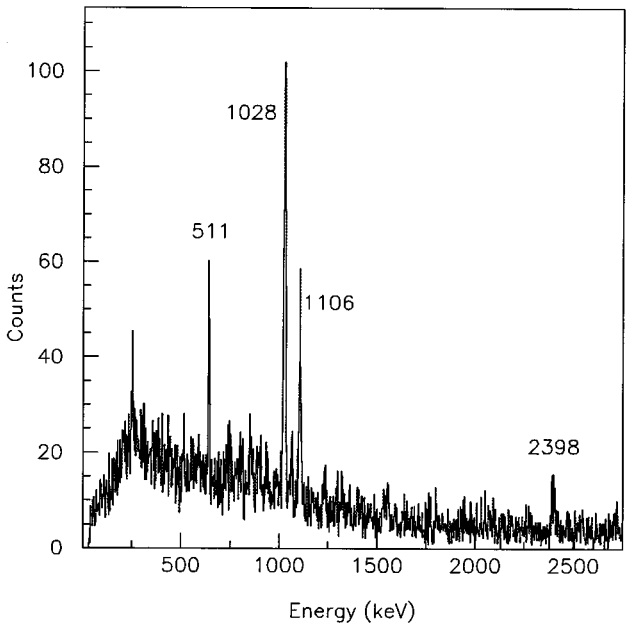

FIG. 2. The summed γ-ray spectrum from the 155° detectors, gated on ^{57}Cu recoil nuclei, after gain matching and Doppler shift corrections have been applied. The small line between the 1028 keV and 1106 keV transitions is the 847 keV line from ^{56}Fe.

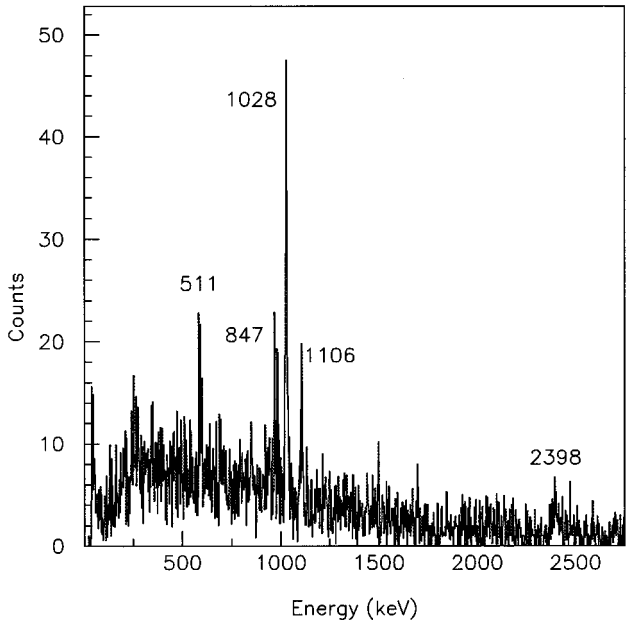

FIG. 3. The summed γ-ray spectrum from the 120° detectors, gated on ^{57}Cu recoil nuclei, after gain matching and Doppler shift corrections have been applied. The 511 and 847 keV lines appear fragmented because the three 120° detectors were not aligned at the same angle, and so they had different Doppler shift factors.

rection factors. The ^{56}Fe line is much weaker in the 155° detectors than at 120° because they were substantially further from the steel plate and quadrupole magnet. We do not see evidence for inelastic neutron scattering on Ge in either of these spectra. This is consistent with the kinematics of the ^{1}H(^{58}Ni,^{57}Cu)2n reaction. The structure observed in Fig. 2 near 250 keV appears to be due to gain-match-related binning, primarily in one of the four 155° Ge detectors. We do not see a line at the corresponding energy in the 120° detectors, and so we conclude that it is not related to any transition in ^{57}Cu. Given the observed ^{57}Cu γ-ray energies, a potential concern is contamination of the 1106 keV line by the 1105.5 keV line in ^{58}Cu leaking through our M/Q gate. As seen in Fig. 1, the 1105.5 keV line is only weakly populated in the $N=Z$ γ-ray spectra. By contrast, the 444.6 keV line, which is in coincidence with this line, is populated strongly in the $N=Z$ spectra and is absent in the ^{57}Cu spectra which were taken concurrently. Thus, we conclude that the 1106 keV line that we observe in ^{57}Cu has negligible contamination from the 1105.5 keV line in ^{58}Cu. Furthermore, the other six strong γ-ray lines that are associated with $N=Z$ nuclei are also absent in Figs. 2 and 3.

The uncertainties for the final ^{57}Cu excitation energies are dominated by the accuracy of the Doppler shift correction factors. Two effects contribute to their uncertainty. The smaller effect arises from the possible variation in the average magnetic rigidities of the ^{54}Co, ^{57}Cu, and ^{58}Cu groups selected by the momentum slit in MARS. Rate determinations as the slit position was moved to each side imply that there is an uncertainty in the ^{57}Cu velocity of at most $\pm 0.4\%$ due to this effect. The larger effect arises from the unknown lifetimes of the various γ-ray transitions, coupled with the unknown distributions of excited states produced as the beam slows while passing through the target. This leads to an uncertainty in the actual ^{57}Cu velocity to use when correcting for Doppler shift — that for a recoil nucleus near the front of the target, for a recoil near the center of the target, or for a recoil in flight beyond the target. The actual Doppler shift factors computed above are consistent with the expected velocity of a ^{57}Cu recoil nucleus in the target at a depth of ≈ 5 mg/cm^2. We estimate that the uncertainty in this velocity is $\pm 2\%$, based on the Q values to populate excited states in ^{57}Cu at the observed energies and the known lifetimes of the low-lying excited states in ^{57}Ni [10]. Given this uncertainty in the Doppler shift corrections, we

TABLE I. Level assignments in ^{57}Cu. All excitation energies are in keV. The ^{57}Ni excitation energies and spin-parity assignments are from Ref. [10]. It has no other known states below 3 MeV.

J^π	^{57}Ni energy	This expt.	Ref. [3]	Ref. [4]	^{57}Cu adopted values
$\frac{3}{2}^-$	g.s.				g.s.
$\frac{5}{2}^-$	768.5	1028(4)	1040(40)	1040(40)	1028(4)
$\frac{1}{2}^-$	1112.6	1106(4)	–	–	1106(4)
$\frac{5}{2}^-$	2443.1	2398(10)	–	–	2398(10)
$\frac{7}{2}^-$	2577.6	–	–	2520(40)	2520(40)

TABLE II. Calculated properties of the resonances in the reaction ^{56}Ni$(p,\gamma)^{57}$Cu. The factors A_i and B_i are defined in Eq. (1).

E_x	$E_{\rm res}$	l	This work				Ref. [1]		Ref. [2]	
keV	keV		Γ_p (eV)	Γ_γ (eV)	A_i	B_i	A_i	B_i	A_i	B_i
1028	333	3	6.1(-13)	3.8(-6)	2.85(-7)	3.86	–	–	9.5(-7)	3.482
1106	411	1	1.5(-8)	1.3(-2)	2.30(-3)	4.77	1.29(-2)	4.90	4.59(-5)	3.482
2398	1703	3	8.5(-2)	2.3(-2)	8.42(+3)	19.76	7.06(+3)	20.33	9.97(+2)	19.75
2520	1825	3	7.0(-2)	1.3(-2)	6.97(+3)	21.18	–	–	8.87(+3)	21.38

adopt 1028 ± 4 keV, 1106 ± 4 keV, and 2398 ± 10 keV as our observed γ-ray energies in ^{57}Cu.

IV. LEVEL ASSIGNMENTS

Table I shows our level assignments for ^{57}Cu. We assume that all three measured γ rays represent transitions from excited states in ^{57}Cu to its ground state. This is consistent with the observation that all states in the mirror nucleus ^{57}Ni below 3.2 MeV have ground state γ-decay branching ratios of $>90\%$ [10]. We have also included the analog states in ^{57}Ni and a comparison of our results to two previous measurements in Table I. The J^π assignments for the ^{57}Cu states are based on our analog assignments and the known mirror states in ^{57}Ni. We conclude that the state which was seen previously at 1040 keV [3,4] was primarily due to the state that we see at 1028 keV, possibly with some contamination by the state that we see at 1106 keV. The state which we see at 2398 keV has not been reported before, while we do not see the state which was reported previously at 2520 keV [4].

The spin and parity of the ^{57}Cu ground state is known to be $\frac{3}{2}^-$ from β-decay studies [8]. Our spin and parity assignments for the 1028 and 1106 keV states are based on several considerations. Both angular momentum matching and statistical weighting would predict that we should populate the analog of the 768 keV $1f_{5/2}$ state in ^{57}Ni more strongly than the analog of the 1113 keV $2p_{1/2}$ state. We find that the yield of the 1028 keV state is 2.6 times larger than that of the 1106 keV state. In Ref. [3], ^{57}Cu was produced in the reaction ^{58}Ni$(^7$Li$,^8$He$)^{57}$Cu at a beam energy of 174 MeV and a scattering angle of 5°. The yield to the excited state at 1040 ± 40 keV was over 3 times larger than that of the ^{57}Cu ground state. One would expect this reaction to populate the $2p_{1/2}$ state somewhat more weakly than the $2p_{3/2}$ ground state, based on their similar structures together with their Q value and statistical weighting differences. Thus, we conclude that most of the yield observed in the previous work must have excited the $1f_{5/2}$ state. Given the good agreement between its excitation energy and the state that we observe at 1028 keV, we conclude that this state must be the analog of the 768 keV $\frac{5}{2}^-$ state in ^{57}Ni. Finally, the assignments of these two states are consistent with theoretical expectations for their relative Coulomb shifts. Finite-well Hartree-Fock calculations, including core polarization effects and corrected to reproduce the rms charge radius of ^{57}Ni [3], predict that the $2p_{3/2}$ and $2p_{1/2}$ states should have essentially identical Coulomb displacement energies in mass 57, since they have the same radial wave functions, while the $1f_{5/2}$ state should lie just below the $2p_{1/2}$ state in ^{57}Cu. This is precisely the pattern that we observe. We find a difference of 260 keV between the Coulomb shifts of the $2p_{3/2}$ and $1f_{5/2}$ proton states, while the Coulomb shifts of the $2p_{3/2}$ and $2p_{1/2}$ states differ by only 7 keV.

Our analog assignments for the 2398 and 2520 keV states are based on a weak coupling model for these states in mass 57 nuclei. In this model, they arise primarily from the coupling of a $2p_{3/2}$ nucleon to the ^{56}Ni 2^+ first excited state. Such states would be expected to have similar Coulomb shifts. These Coulomb shifts would also be expected to be similar to those of the essentially single-particle $2p_{3/2}$ ground state and $2p_{1/2}$ second excited state. Given our spin assignments, we find relative Coulomb shifts of only 45 ± 10 keV and 57 ± 40 keV for these two states.

V. ^{56}Ni$(p,\gamma)^{57}$Cu REACTION RATE

Except at the highest temperatures, the main path of the rp process passes through ^{56}Ni [1,2], which is more bound and has a longer lifetime than any of its neighbors due to its doubly magic structure. These properties make it a waiting point in the reaction network. The production of heavier nu-

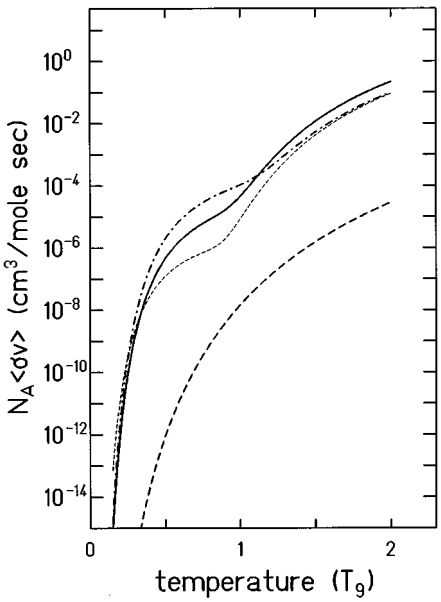

FIG. 4. The resonant reaction rate for the proton radiative capture reaction ^{56}Ni$(p,\gamma)^{57}$Cu versus temperature, calculated with the data in Table II. The solid curve shows the results of this work. For comparison, the dot-dashed curve shows the rate assumed in Ref. [1], and the short dashed curve shows that assumed in Ref. [2]. The long dashed curve shows the nonresonant contribution [2].

clei is therefore determined by the rate of the radiative proton capture reaction $^{56}\mathrm{Ni}(p,\gamma)^{57}\mathrm{Cu}$. The proton separation energy of ^{57}Cu is only $S_p = 695 \pm 20$ keV [3,4,11], and so all of its excited states are resonances in this reaction. For separate narrow resonances, the temperature-averaged resonant reaction rate in a stellar environment can be written as

$$\lambda = N_A\langle\sigma v\rangle = N_A\left(\frac{2\pi}{\mu kT}\right)^{3/2}\sum_{\text{res}} \omega\frac{\Gamma_p\Gamma_\gamma}{\Gamma_p+\Gamma_\gamma}\exp\left(-\frac{E_R}{kT}\right) = T_9{}^{-3/2}\sum_i A_i\exp\left(-\frac{B_i}{T_9}\right), \quad (1)$$

where ω is the statistical weight factor, Γ_p and Γ_γ are the proton- and gamma-decay widths of the ith resonance of energy E_R, and T_9 is the temperature in units of 10^9 K.

We use the excitation energies from the present experiment to determine the resonance locations and a description of the low-lying excited states in ^{57}Cu using a version of the extended unified model (EUM) [12] to estimate their decay widths. This description treats the low-lying states in ^{57}Cu as mixtures of pure single-particle states outside the doubly closed shell ^{56}Ni core and collective excitations of the core coupled to the same single-particle states. In particular, the 2^+ first excited state of ^{56}Ni at 2701 keV has the features of a quadrupole vibration and is at an energy comparable to the single-particle excitations. Consequently the residual particle-core interaction leads to configuration mixing between the single-particle and the core-coupled configurations which affects the purity of the expected single-particle states. The procedure follows closely that used in a recent study of the single-particle energies in $N=83$ nuclei [13].

First, we used the model to describe the low-lying states in ^{57}Ni for which more data exist. Then we performed calculations for ^{57}Cu using the same procedure and parameters, except for the single-particle energies which are different due to the Coulomb displacement. The only core-coupled configurations that play a significant role for the ^{57}Cu states of interest are $[^{56}\mathrm{Ni}(2^+)\times 2p_{3/2}]_{1/2,3/2,5/2,7/2}$. The EUM introduces the coupling between the odd nucleon and the core excitations via a particle-vibration coupling Hamiltonian [14]. The quadrupole coupling strength was determined from the recently measured $B(E2)$ for the ^{56}Ni first excited state [15]. To reproduce the observed spin order and energy splitting for the quadrupole multiplet in the mirror ^{57}Ni, we used the interaction between the quadrupole moment of the core state and that of the single particle. A value $Q_m(2^+)=10$ fm^2 for the isoscalar (mass) quadrupole moment of the core state was used. This is the only free parameter in the calculations. The resulting excitation energies for ^{57}Ni and ^{57}Cu agree with the known states. Lifetimes of the low-lying states in ^{57}Ni also compare well with the known values [10] if the neutron effective charge and spin g factor are taken to be $e_{\text{eff}}=0.6e$ and $g_{\text{eff}}=0.6g_{\text{bare}}$. The only significant deviation from experiment is for the lifetime of the $\frac{5}{2}^-$ first excited state, which is known to have a large ℓ-forbidden $B(M1)$ [10] that is not reproduced by the EUM calculations.

Using the calculated wave functions for ^{57}Cu, we determine proton decay widths for the lowest four resonances as

$$\Gamma_p(E,l) = \left(\frac{2E}{\mu}\right)^{1/2} P_l(E_r,R_n)C^2_{\text{s.p.}}\chi^2_{nlj}(R_n), \quad (2)$$

where $C^2_{\text{s.p.}}$ is the square of the coefficient of the single-particle component in the wave function (the spectroscopic factor), $\chi_{nlj}(R_n)$ is the single-particle radial wave function of the (nlj) orbital at the nuclear radius R_n, and $P_l(E_r,R_n)$ is the barrier penetration factor. In particular, we find that the spectroscopic factors $C^2_{\text{s.p.}}$ are 0.87, 0.76, and 0.028 for the first three resonances. The $\frac{7}{2}^-$ resonance has no proton width within this limited model space since there is no free single-particle orbital available for mixing. In the results below, we have taken $C^2_{\text{s.p.}}$ to be 0.01 for this state to simulate the contribution from additional configuration mixing outside our model space. The same EUM wave functions and an electromagnetic transition operator with the $E2$ collective part from the core nucleus and a proton single-particle effective charge $e_{\text{eff}}=1.3e$ were used for the calculation of the γ-decay widths. Further details regarding the EUM calculations, including their implications for the Coulomb displacement energies in $A=57$, will be the subject of a future publication.

Our results are summarized in Table II in the form of the resonance energies, proton- and gamma-decay widths, and the coefficients A_i and B_i defined in Eq. (1). They are compared with the resonance properties assumed in Refs. [1,2]. Figure 4 shows the calculated stellar reaction rate versus temperature in the range up to $T_9=2.0$. For temperatures below $T_9=0.1$, the first resonance dominates due to its proximity to the reaction threshold, but its $l=3$ character makes it very weak. This resonance was neglected in Ref. [1]. Although it was included in Ref. [2], it made a negligible contribution compared to the $l=1$, $J^\pi=\frac{1}{2}^-$ resonance, because the two resonances were assumed to be degenerate. We find that the $\frac{1}{2}^-$ resonance dominates for $T_9=0.1$ to $T_9=1.0$, where the second $\frac{5}{2}^-$ resonance becomes more important in spite of its rather small spectroscopic factor. The contribution from the $\frac{7}{2}^-$ resonance, although significant at high temperatures, never equals that from the $\frac{5}{2}^-$ resonance. There is an additional contribution to the stellar $^{56}\mathrm{Ni}(p,\gamma)^{57}\mathrm{Cu}$ reaction rate from direct capture, which was estimated in Ref. [2]. However, it is at least three orders of magnitude smaller than the resonant contribution over the entire temperature range considered here.

An examination of the calculated resonance properties in Table II indicates that $\Gamma_p \ll \Gamma_\gamma$ for the first two resonances, and so the predicted values of Γ_p dominate the uncertainty in the contributions that these two make to the astrophysical reaction rate. Since both of these are reasonably pure single-particle states with large spectroscopic factors, the 20 keV uncertainty in the ^{57}Cu proton separation energy makes the largest contribution to the uncertainties in Γ_p for them. In

particular, 20 keV shifts in S_p change the A_i coefficients for the first two resonances by factors of 4.4 and 2.8, respectively, about their central values. These effects are partially compensated by the corresponding changes in the B_i coefficients, leading to an overall uncertainty in the reaction rate of a factor of 2 for $T_9 \approx 0.7$. For the upper two resonances, we predict that $\Gamma_\gamma < \Gamma_p$, making the contribution of these states to the reaction rate sensitive to the calculated values of Γ_γ and relatively insensitive to the presumed values of Γ_p. The EUM calculations of the lifetimes of the ^{57}Ni analogs for these two states agree with their experimental values to within 20%, demonstrating that their gamma widths are estimated reliably. By contrast, the small proton spectroscopic factors for these two levels mean their proton widths are sensitive to the details assumed in the nuclear structure calculations. Indeed, the fact that we observe the γ decay of the 2398 keV state and do not see evidence for the 2520 keV state implies that we have likely underestimated the proton spectroscopic factor of the $\frac{7}{2}^-$ state and, hence, overestimated its γ-decay branching ratio. An alternative explanation of the fact that we see the 2398 keV state and not the 2520 keV state is that their spin assignments could be reversed, which would simultaneously increase the predicted γ-decay branching ratio of the 2398 keV state and decrease the branching ratio for the 2520 keV state. We consider this scenario to be very unlikely, given the Coulomb systematics discussed in Sec. IV. However, it would have very little impact on our calculated stellar reaction rate in any case. Reversing the spin assignments for these two states would have a negligible effect on the stellar reaction rate for $T_9 < 1.0$ and would reduce our predicted reaction rate by $\leqslant 20\%$ for $T_9 > 1.0$. We estimate that the overall uncertainty in our predicted reaction rate is no more than 40% for $T_9 > 1.0$. Figure 5 shows the uncertainty in our calculated stellar reaction rate vs temperature.

As seen in Fig. 4, we find that the ^{56}Ni$(p,\gamma)^{57}$Cu reaction rate falls between those assumed in Refs. [1,2] for temperatures $T_9 = 0.35 - 1.1$ and is a factor of ≈ 2 larger at high temperatures. Clearly, the most significant deviations between our results and the previous reaction network calculations occur in the temperature range which is dominated by the $2p_{1/2}$ second excited state in ^{57}Cu. The primary difference between our result and Ref. [1] originates in the somewhat smaller Γ_p that we assume for the $2p_{1/2}$ state due both to a slight shift in the resonance energy and a more realistic calculation of the decay width. The difference between our result and Ref. [2] stems from its dependence on Ref. [3] to determine the resonance energy of the $2p_{1/2}$ state. Given the higher excitation energy that we find for this state and the smaller present value of the ^{57}Cu proton separation energy [3,4,11] than assumed in Ref. [3], we find the astrophysical reaction rate is a factor of ≈ 8 larger at intermediate temperatures than assumed in Ref. [2]. This may permit the rp process to produce significant yields of nuclei beyond the iron region at substantially lower temperatures than implied by the recent reaction network predictions.

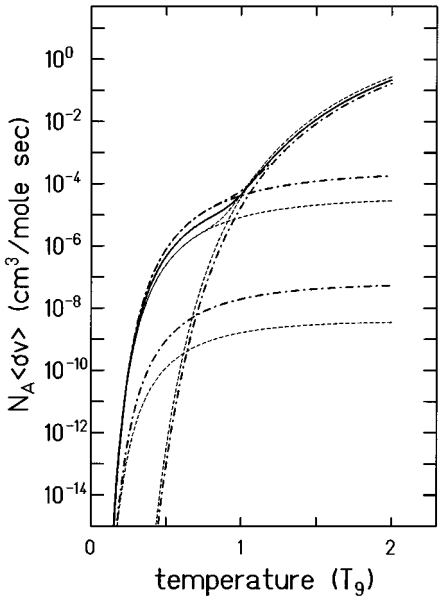

FIG. 5. The uncertainty in the calculated ^{56}Ni$(p,\gamma)^{57}$Cu stellar reaction rate versus temperature. The solid line shows the calculated rate, with the band around it indicating the uncertainty, as discussed in the text. Contributions from the 1028 keV state, the 1106 keV state, and the sum of the 2398 and 2520 keV states are also shown separately as individual bands.

In conclusion, we have observed the first three excited states of ^{57}Cu in the reaction ^{1}H(^{58}Ni,^{57}Cu-γ)$2n$ and assigned their spins and parities by correlating them to known analog states in the mirror nucleus ^{57}Ni. We have used a simple model to estimate the proton- and gamma-decay widths of these states. Finally, we have combined these results to calculate the astrophysical rate for the reaction ^{56}Ni$(p,\gamma)^{57}$Cu, which plays a central role in the production of nuclei beyond $A = 56$ via the rp process.

ACKNOWLEDGMENTS

We would like to thank F. Stephens of Lawrence Berkeley Laboratory for his assistance in the loan of the Compton-suppressed Ge detectors from the HERA array and C. Baktash of Oak Ridge National Laboratory for the loan of much of the electronics that was used to instrument them. This research was supported in part by the U.S. Department of Energy under Grant No. DE-FG03-93ER40773, by the U.S. National Science Foundation under Grant No. PHY-9215014, and by the Robert A. Welch Foundation.

[1] R.K. Wallace and S.E. Woosley, Astrophys. J. Suppl. **45**, 389 (1981).

[2] L. Van Wormer, J. Gorres, C. Iliadis, M. Wiescher, and F.-K. Thielemann, Astrophys. J. **432**, 326 (1994).

[3] B. Sherrill, K. Beard, W. Benenson, C. Bloch, B.A. Brown, E. Kashy, J.A. Nolen, Jr., A.D. Panagiotou, J. van der Plicht, and J.S. Winfield, Phys. Rev. C **31**, 875 (1985).

[4] E. Stiliaris, H.G. Bohlen, X.S. Chen, B. Gebauer, A. Miczaika,

W. von Oertzen, W. Weller, and T. Wilpert, Z. Phys. A **326**, 139 (1987).
[5] R.E. Tribble, R.H. Burch, and C.A. Gagliardi, Nucl. Instrum. Methods A **285**, 441 (1989).
[6] R.E. Tribble, C.A. Gagliardi, and W. Liu, Nucl. Instrum. Methods B **56/57**, 956 (1991).
[7] Micron Semiconductor, Inc.
[8] D.R. Semon, M.C. Allen, H. Dejbakhsh, C.A. Gagliardi, S.E. Hale, J. Jiang, L. Trache, R.E. Tribble, S.J. Yennello, H.M. Xu, X.G. Zhou, and B.A. Brown, Phys. Rev. C **53**, 96 (1996).
[9] R.M. Diamond, in *Instrumentation for Heavy Ion Nuclear Research*, edited by D. Shapira (Harwood Academic, New York, 1985), p. 259.
[10] M.B. Bhat, Nucl. Data Sheets **67**, 195 (1992).
[11] C.A. Gagliardi, D.R. Semon, R.E. Tribble, and L.A. Van Ausdeln, Phys. Rev. C **34**, 1663 (1986).
[12] L. Trache, K. Heyde, and P. von Brentano, Nucl. Phys. **A554**, 118 (1993).
[13] L. Trache, A.M. Oros, P. von Brentano, G. Graw, and K. Heyde, Phys. Scr. T **56**, 292 (1995).
[14] A. Bohr and B. Mottelson, *Nuclear Structure* (Benjamin, Reading, MA, 1975), Vol. 2, p. 325.
[15] G. Kraus *et al.*, Phys. Rev. Lett. **73**, 1773 (1994).